ChemPubSoc Europe

DOI: 10.1002/cbic.201800122

CHEMBIOCHEM Communications

Construction of a Holliday Junction in Small Circular DNA Molecules for Stable Motifs and Two-Dimensional Lattices

Xin Guo,[a] Xue-Mei Wang,[a] Shuai Wei,[b] and Shou-Jun Xiao*[a, c]

Design rules for DNA nanotechnology have been mostly learnt from using linear single-stranded (ss) DNA as the source material. For example, the core structure of a typical DAO (double crossover, antiparallel, odd half-turns) tile for assembling 2D lattices is constructed from only two linear ss-oligonucleotide scaffold strands, similar to two ropes making a square knot. Herein, a new type of coupled DAO (cDAO) tile and 2D lattices of small circular ss-oligonucleotides as scaffold strands and linear ss-oligonucleotides as staple strands are reported. A cDAO tile of cDAO-c64nt (c64nt: circular 64 nucleotides), shaped as a solid parallelogram, is constructed with a Holliday junction (HJ) at the center and two HJs at both poles of a c64nt; similarly, cDAO-c84nt, shaped as a crossed quadrilateral composed of two congruent triangles, is formed with a HJ at the center and four three-way junctions at the corners of a c84nt. Perfect 2D lattices were assembled from cDAO tiles: infinite nanostructures of nanoribbons, nanotubes, and nanorings, and finite nanostructures. The structural relationship between the visible lattices imaged by AFM and the corresponding invisible secondary and tertiary molecular structures of HJs, inclination angle of hydrogen bonds against the double-helix axis, and the chirality of the tile can be interpreted very well. This work could shed new light on DNA nanotechnology with unique circular tiles.

Since Seeman's pioneering work on DNA nanotechnology in the early 1980s, DNA molecules have been used to build fascinating motifs for the construction of many kinds of nanostructures. Typical motifs include DAE (double crossover, antiparallel, even half-turns; often 4 and 6) and DAO (double crossover, antiparallel, odd half-turns; often 5) tiles,[1] star tiles,[2] single-stranded (ss) tiles and ss-bricks,[3] and DNA origami.[4] Among most of the DNA nanostructural assemblies, Holliday junctions (HJs)[5] play key roles as pivot points for crosslinking four double-stranded (ds) arms and intensifying the rigidity of DNA motifs and lattices.[1b] To date, most DNA motifs and lattices have been assembled from linear ssDNAs as the source materials. However, both linear and circular DNAs are widely distributed in biological species, playing a central role in gene replication, transcription, recombination, translation, protein recognition, and so forth. Topological differences in DNA will differentiate the secondary and tertiary structures of key biological elements, such as HJs, in terms of conformation, chirality, supercoiling, condensation, and so forth, as well as in their biological functions.

Recently, a few reports have described the use of circular ss-oligonucleotides as scaffolds to build motifs, nanotubes, and DAE lattices.[6] For conciseness, we define a "circular tile" as a stable DNA complex molecule associated with one circular scaffold and other linear staples of ss-oligonucleotides, whereas a "linear tile" results from a full set of linear ss-oligonucleotides.

The following differences can be observed in DNA nanotechnology for the same design, but with circular tiles instead of linear tiles: 1) A circular DNA molecule is covalently connected continuously; thus circular tiles and lattices are intensified, relative to linear ones with more nicks. This phenomenon has been observed previously by means of both pre- and post-circularization.[1c,6d–f,7] 2) A circular scaffold can only be threaded by linear staples during assembly to form motifs and to weave lattices, that is, a circular molecule lacks the active twisting spatial degree of freedom and only possesses the adaptive one, whereas a linear molecule has both. From knowledge of the *anti*, eclipsed, and *gauche* conformations of hydrocarbon molecules, to complete such a threading, every nucleotide in a circular strand should rotate freely along its backbone under certain conditions, such as higher temperature; otherwise, the circular strand will be twisted to a high degree of tension that cannot be released, and thus, fully twisted threading cannot be completed. For this reason, patience should be applied to control the sequential dynamic assembly process carefully to avoid the incomplete threading of circular strands. For example, c64nt will be threaded by its complementary linear staple six times, and c84nt by its linear partner staple eight times, after complete association. 3) A molecular crowding environment will exist inside small circular DNA.[8] In other words, bond lengths and angles inside the circle will be smaller than those outside the circle. However, such geometrically crowded structures in circular tiles might not be so different from those of linear tiles because the looped linear scaffold resembles the geometrical shape of the circular tile. The above subtle differences cannot be distinguished in some motifs and their assemblies, such as DAE tiles with E at four or six half-turns and 2D DAE-O (-O indicates an odd half-turns intertile distance) lattices, regardless of if they are circular or linear tiles. For other

[a] *X. Guo, X.-M. Wang, Prof. Dr. S.-J. Xiao*
State Key Laboratory of Coordination Chemistry
School of Chemistry and Chemical Engineering, Nanjing University
163 Xianlin Avenue, Nanjing 210023 (P.R. China)
E-mail: sjxiao@nju.edu.cn

[b] *Dr. S. Wei*
Department of Chemistry, University of Michigan
Ann Arbor, Michigan 48109 (USA)

[c] *Prof. Dr. S.-J. Xiao*
State Key Laboratory of Bioelectronics, Southeast University
Nanjing 210096 (P.R. China)

Supporting information and the ORCID identification numbers for the authors of this article can be found under https://doi.org/10.1002/cbic.201800122.

motifs, subtle geometrical structural differences will be accumulated and magnified in the DNA assemblies, thus resulting in partly or completely different DNA lattices in terms of structure, size, and appearance.

The previously reported circular DAE is structurally similar to a linear DAE, with a negligible difference: the former has a continuous circular scaffold, whereas the latter has a looped scaffold carrying a nick.[6e] What about building a DAO tile from a small circular strand? It seems impossible because the core structure of DAO is composed of only two linear scaffolds, similar to two ropes making a square knot, in which each scaffold makes a U-turn at one crossover and moves in and out of the DAO loop at the other crossover, whereas a circular scaffold restrains its extension out of the scaffold loop at both crossovers. Such a dilemma can be solved by inserting a HJ at the center of c64nt because then a pair of two coupled DAO (cDAO) tiles can be formed by making two additional polar HJs at both poles. This new cDAO motif and its derivatives are stable and rigid enough to assemble 2D DNA lattices up to 5 μm long, whereas the linear cDAO tiles with the same sequence and structure cannot.

We previously reported the use of c64nt as a scaffold to assemble DNA nanotubes.[6d] Continuing this work, we placed a HJ at the center of c64nt and set central symmetric nick pairs at different positions of the two main staples (Figure S4 in the Supporting Information). We found structural polymorphism of annealed mono- and polymers, of which the monomers could be used as rigid motifs for assembling DNA lattices. Schematic double-helical drawings of key circular monomer motifs and polymers are shown in Figure 1. c64bp and c84bp are two control samples, each of which is considered to be a continuous ds loop with a nick at any site of its staple. We illustrate phase analysis for HJ-c64nt, HJ-c84nt, and tHJ-c84nt as examples. Other phases of the motifs can be easily analyzed in the same way.

Because we only deal with 2D nanostructures herein, we discuss the helical phases in the plane of the page. Projection of all nucleotides of a ds-DNA to this plane will generate two sinusoids along the helical axis with an angular phase difference of about 180°. The coordinates of base pairs, nicks, HJs, and three-way junctions are defined according to the number segments in Figure 1. As shown in HJ-c64nt, a central HJ is located at the c64nt center, with coordinates of (16, 17, 16′, 17′), and two nicks at both poles. The four HJ-making nucleotides of the two main staples must locate at the minima and maxima of their own sinusoids nearby relative to the upper and lower helical axes, respectively, inside the c64nt loop. To meet the Watson–Crick helical phasing criteria for a 16 bp distance, each main staple must travel along its sinusoid in and out of c64nt at the same pole from the maxima to the minima or vice

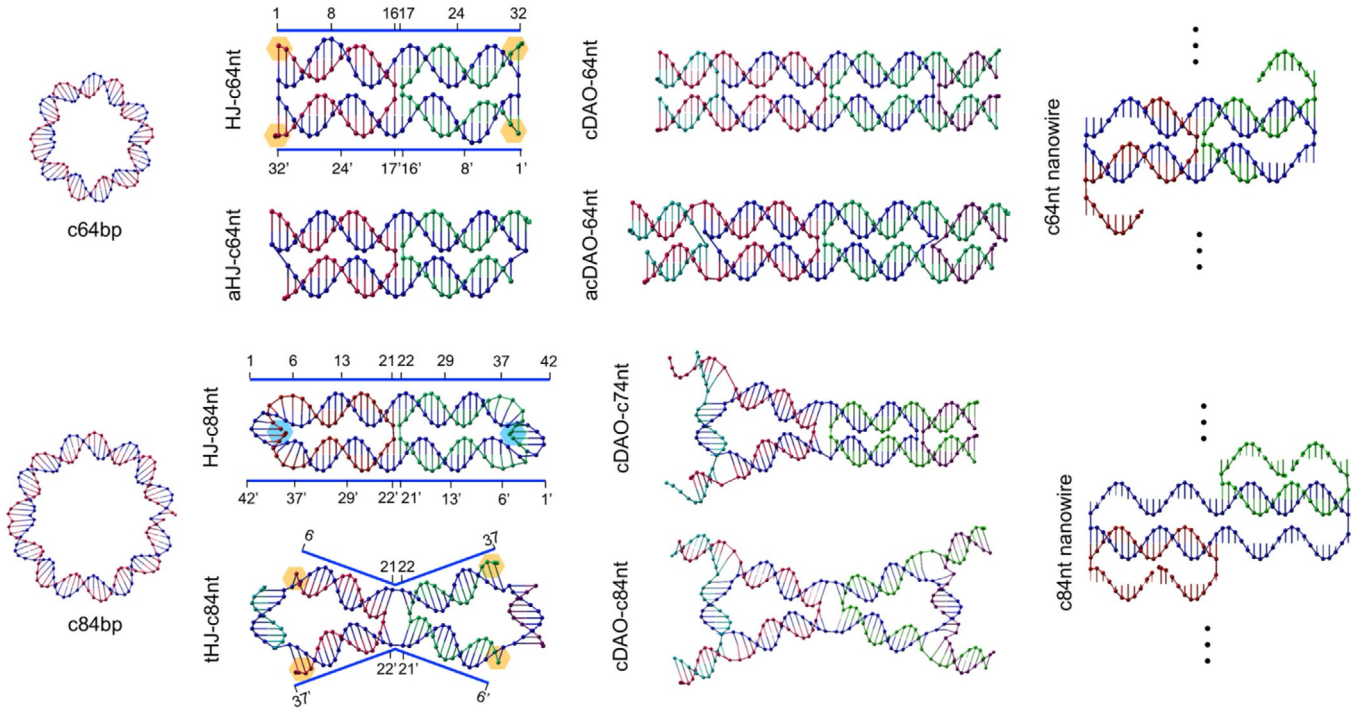

Figure 1. Schematic double-helical models of circular monomer tiles of c64bp, c84bp, HJ-c64nt, aHJ-c64nt, HJ-c84nt, tHJ-c84nt, cDAO-c64nt, acDAO-c64nt, cDAO-c74nt, cDAO-c84nt, as well as polymers of c64nt and c84nt nanowires. Both c64nt and c84nt nanowires are represented as their simplest folding unit cells, in which the three aligned dots above and below each of the two unit cells indicate the infinite alignment of unit cells vertically up and down, with equal distances between duplexes to form nanowires. Double straight and folded number segments with key ordinals in bright blue above and below HJ-c64nt, HJ-c84nt, and tHJ-c84nt indicate sequential base pairs in the upper and lower duplexes of the circular scaffold. In each tile of the second and third columns, the circular scaffolds of c64nt, c74nt, and c84nt are colored deep blue; two main staples that form the central HJ are colored emerald green in the right-half and maroon in the left-half. In each tile of the third column, two helper staples that construct the polar junctions at both ends of the tile are colored auburn in the right-half and olive green in the left-half.

versa; these are labeled with yellow hexagons at positions 1′ and 32 of the right-hand pole and at 1 and 32′ of the left-hand pole in Figure 1. The circular tile of cDAO-c64nt can be easily constructed by extending the two main staples outside both poles of HJ-c64nt to make two extra polar HJs and to associate with two helper staples.

The asymmetric tile of aHJ-c64nt, a twin tile of HJ-c64nt, is composed of 34 bp at the upper strand and 30 bp at the lower strand. Similar to cDAO-c64nt built from HJ-c64nt, the asymmetric acDAO-c64nt is derived from aHJ-c64nt. Although the c64nt nanowire was designed as a monomer (Figure S4), with two central symmetric nicks at (8, 9) of the upper strand and (8′, 9′) of the lower strand, it is actually folded into nanowires, which are schematically drawn in Figures 1 and S6 with a full set of sequences repeated twice. For HJ-c84nt, the helical phasing of the central HJ, with coordinates of (21, 22, 21′, 22′), requires the four HJ-making nucleotides of the two main staples to be at the minima and maxima of their own sinusoids nearby relative to the upper and lower helical axes, respectively, inside the c84nt loop. Due to the routing distance of two full turns of 21 bp, each main staple must come from and go to the same extreme point nearby relative to its helical axis at the same pole inside the c84nt loop, forming a nick labeled with a sky-blue hexagon. Because the two main staples cannot protrude out of c84nt for tile connections, HJ-c84nt cannot be used to assemble 2D lattices.

An alternative path for the two main staples routing out of c84nt is shown in tHJ-c84nt. Each main staple must travel in and out of c84nt, at a 16 bp distance from the central HJ, from the maxima to the minima along its sinusoid or vice versa; these are labeled with four yellow hexagons at positions 6′ and 37 of the right-hand side, and at 6 and 37′ of the left-hand side in Figure 1; both helper staples associate with the remainder of the two 10 nt segments of 38-to-5′ and 5-to-38′, respectively. This folding strategy makes a crossed quadrilateral composed of two congruent triangles. cDAO-c84nt can be easily constructed by extending the main and helper staple strands out of tHJ-c84nt and pairing correlated strands. cDAO-c84nt is so called because the four three-way crossovers (or three-way junctions) at the four corners, with coordinates of (37, 38), (5′, 6′), (37′, 38′), and (5, 6), are coupled together through the central four-way crossover (central HJ). cDAO-c74nt is folded such that half is a solid parallelogram, similar to half of cDAO-c64nt, and half is a hollow triangle, similar to half of cDAO-c84nt. Similar to the c64nt nanowire, the c84nt nanowire was designed as a monomer with two central symmetric nicks at (10, 11) of the upper strand and (10′, 11′) of the lower strand, but it is actually folded as nanowires; these are schematically drawn in Figures 1 and S7 with a full set of sequences repeated twice.

Native PAGE is the primary experimental method used to examine stable DNA molecules as motifs or tiles for DNA nanotechnology (Figure 2A; sample names are listed at the top). We explain the PAGE results through the well-known DNA reptation model in electrophoresis.[9] The linear ds-helix can be pictured as moving through impenetrable gel fibers, with the motion mediated by a snake-like reptation; the circular ds-helix in our case should be modified by the number and size of pores found within. Four fully associated c64nt duplexes with designed nick(s) on staples were run in the four left-hand lanes. c64bp migrated as a wriggling oblong loop with a medium-sized pore inside, in which the pore was penetrated by gel fibers; thus c64bp was retarded to a band corresponding to a linear 74 bp marker. HJ-c64nt can be pictured as a wriggling lanky Arabic number 8, with two small-sized pores, whereas aHJ-c64nt, with a similar shape to that of HJ-c64nt, is bent somehow towards the short 30 bp side. Their migration bands correspond to a linear 64 bp marker. The migration band of the c64nt nanowire is at the slot entrance; this indicates that it is a polymer and not a monomer, as designed. The c64nt nanowire was also imaged by AFM (Figure 2C).

We have investigated a series of central symmetrical nick pairs with coordinates from {(2, 3), (2′, 3′)} to {(14, 15), (14′, 15′)} by native PAGE (Figure S4). Among all nick pairs, only three {(32′, 1), (32, 1′)}, {(1, 2), (1′, 2′)}, and {(2, 3), (2′, 3′)} pairs

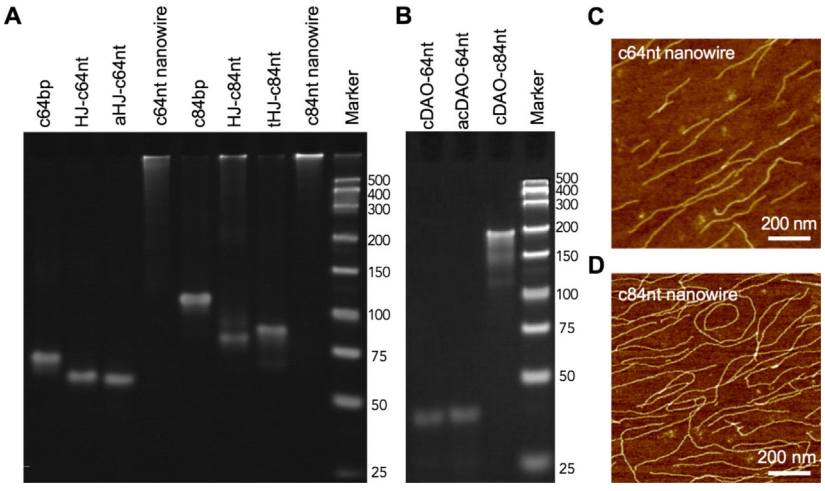

Figure 2. A) and B) Photographs of native PAGE gels of DNA motifs with sample names listed above each lane, and AFM images of C) c64nt and D) c84nt nanowires.

close to both poles at balanced positions presented stable monomer tiles, such as HJ-c64nt; the {(3, 4), (3′, 4′)} pair gave an unknown intermediate monomer, corresponding to a linear 140 bp marker, which could be explained by migration retardation of two larger pores; the eight {(4, 5), (4′, 5′)} to {(11, 12), (11′, 12′)} pairs, away from the three balanced positions, generated polymers to avoid torsional and shear stresses; and the final three {(12, 13), (12′, 13′)} to {(14, 15), (14′, 15′)} pairs close to the center provided monomers with similar shapes and migrational behavior to c64bp, thus indicating that they did not form a central HJ.

Four fully associated c84nt duplexes with designed nick(s) on staples were run in the four right-hand lanes beside the markers (Figure 2A). c84bp, similar to c64bp, but with a large-sized pore, was penetrated and retarded by massive gel fibers and migrated much more slowly with a band corresponding to a linear 130 bp marker. HJ-c84nt, similar to HJ-c64nt, but with two slightly larger pores inside and two nicks at both poles, has a clear band, corresponding to a linear 84 bp marker, which indicates a monomer, whereas a slot entrance band also shows other conformers because even stable HJ-c84nt (Figure 1) could possess some strain as a result of insufficient base pairing at both poles. The stable triangular tile of tHJ-c84nt without overhangs is proven by a clear band corresponding to a linear 90 bp marker. The c84nt nanowire is confirmed to be a polymer, with a band at the slot entrance. The nanowire structure is also confirmed by AFM (Figure 2D). The c64nt nanowire is straighter and shorter than that of the c84nt nanowire, due to a central HJ in c64nt. Although both c64nt and c84nt nanowires could have other folding structures, such as nanotubes,[6d] they are assigned as nanowires because heights in air determined by AFM imaging were measured to be only 1.2 nm.

In Figure 2B, the three assemblies of cDAO-c64nt, acDAO-c64nt, and cDAO-c84nt, each carrying four 10 bp blunt-ended overhangs, are proven to be stable monomer tiles, respectively, with each assembly presenting only one clear band. Both cDAO-c64nt and acDAO-c64nt of 104 bp ran much faster on the PAGE gel, corresponding to a linear 42 bp marker; this can be explained by a reptation model as a straight and tight rod without inner pores. Their high rigidity is attributed to the synergistic effect of three HJs in combination, as proven by the lattice appearances and persistence length calculations (see below). cDAO-c84nt migrated as a linear 190 bp marker much more slowly than its precursor tHJ-c84nt tile. Such a huge retardation effect can be interpreted by the four 10 bp overhangs, which increase the tile volume greatly.

Tile stability can be well illustrated by a clear band in the native PAGE gel, whereas tile rigidity cannot be correlated to the migration distance in a straightforward way. The relationship between rigidity and migration distance of a tile is complicated by tile geometries, such as the skeleton, for example, a solid rod of (a)cDAO-c64nt or the hollow integral rigid frame of cDAO-c84nt; number of pores and sizes; and occupied volume.

The 2D infinite lattices assembled from two-tile systems of cDAO-c64nt-E and cDAO-c64nt-O are shown in Figure 3A and B, respectively, as AFM images, and in Figure 3E and F, respectively, as the corresponding schematic assembling models. cDAO-c64nt-E and cDAO-c64nt-O differ by the intertile distances; -E indicates even numbers of four half-turns, and -O indicates odd numbers of five half-turns. The former requires all tiles to be aligned identically; thus all c64nt scaffolds rotate in the same direction, as indicated by the curved arrows in Figure 3E. The latter, with the schematic assembly model shown in Figure 3F, requires alternation of the faces of two neighboring tiles along the horizontal helical axes. The cDAO-c64nt tile core of the solid parallelogram has twofold symmetry; thus the rotation directions of the two horizontal neighboring c64nt scaffolds are opposite, whereas alignment of the tiles along

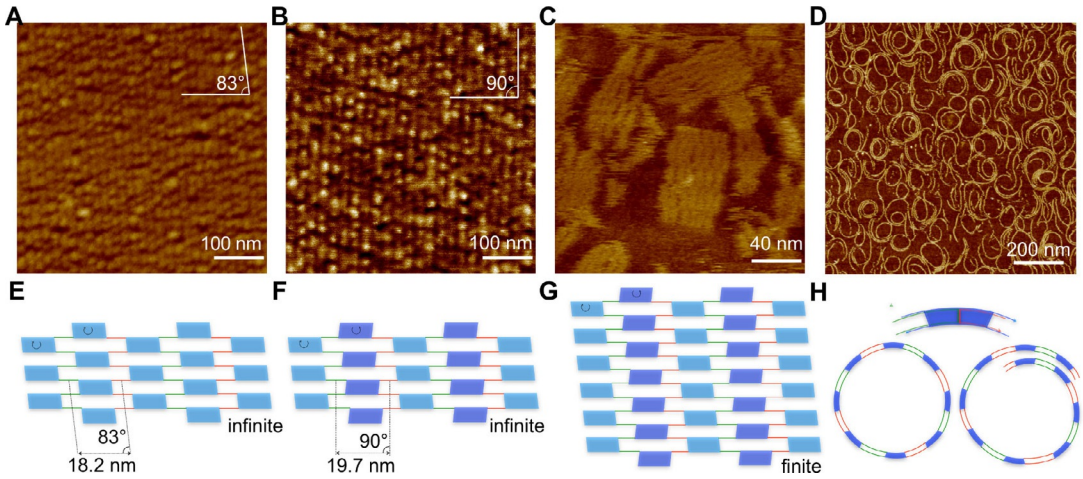

Figure 3. AFM images of A) infinite cDAO-c64nt-E, B) infinite cDAO-c64nt-O, C) finite 5×6 patches of cDAO-c64nt-O, D) infinite acDAO-c64nt-E, and their corresponding schematic assembly models (E–H). In the schematic assembly models, the cDAO-c64nt tile core with a twofold symmetry is represented by a solid parallelogram and its two different faces are distinguished as sky blue and deep blue in (E)–(G); the intertile connections are drawn as red and green segments; and the acDAO-c64nt tile core is drawn as a solid reverse trapezoid colored deep blue in (H). Curved arrows in (E)–(G) point to the rotation direction of circular scaffolds, respectively. The lattice parameters are labeled on the assembly models of (E) and (F), respectively. Schematic parallelogram tiles of cDAO-c64nt from (E) to (G) are aligned with their longitudinal axes to the horizontal.

the vertical arrays remains the same; such a cDAO-c64nt-O assembly follows the "corrugation rule".[2e] Both assemblies yield planar nanoribbons. The cDAO-c64nt-E ribbon is 1.2 nm high, 2.0 μm wide, and 5.0 μm long (Figures 3A and S19), and the cDAO-c64nt-O ribbon is 1.2 nm high, 0.6 μm wide, and 5.0 μm long (Figures 3B and S20). The indented parallel stripes are located at the sticky-end cohesion regions, which are about 1.7 nm wide, that is, 5 to 6 bp long. The periodic distances of the stripes for cDAO-c64nt-E and cDAO-c64nt-O are 18.2 and 19.7 nm, respectively; these values are in agreement with those determined theoretically: $(32+21)\,bp\times0.34\,nm\,bp^{-1}=18.0$ nm and $(32+26)\,bp\times0.34\,nm\,bp^{-1}=19.7$ nm, respectively, if we assign a rise of 0.34 nm per base pair.

The linear DAE-E system was reported to yield nanotubes because the four half-turns intertile distance requires the curved DAE tiles to be aligned identically, which led to closing of a patch of tile arrays to form a nanotube.[10] The planar nanoribbons from cDAO-c64nt-E exclude tile curvature and confirm our previous claim that cDAO-c64nt behaves as a straight and tight rod and is much more rigid and planar than linear DAE tiles with E=4 or 6. From the tile rigidity and the densely woven texture of cDAO-c64nt-E lattices, the helical axes can be assigned to follow the longitudinal axis of the ribbon; thus a tilt angle of 83° of the stripes with respect to the helical axes was measured. A chiral model of cDAO-c64nt is suggested according to inclination of base-paired hydrogen bonds versus the double-helical axis, which was reported previously in HJ-related DNA single crystals[11,5d] and in an RNA assembly system.[12] The tilt angle of 83° is attributed to the synergistic effect of a combination of three HJs of cDAO-c64nt. The absolute tile conformation or chirality in Figure 3E can be aligned directly to the lattice image in Figure 3A.

For the cDAO-c64nt-O ribbon, the parallel stripes were measured to be perpendicular to the longitudinal axis of the ribbon, that is, the helical axes (Figure 3B, F). The perpendicular structure is explained by the assembly model with a staggered arrangement of chirality-alternating tiles along the helical axes. In this case, both upper and lower surfaces of a ribbon are structurally equal. We also designed a finite lattice of 5×6 patches of cDAO-c64nt-O (Figure 3C, G), including 32 tiles with the same circular scaffold of c64nt and differently sequenced overhangs (Figure S14). All four edges of the finite lattice have six thymine-ending overhangs to prevent interlattice π–π edge stacking.[3a,b] The lattice was about 82 nm long and about 40 nm wide, which corresponded to theoretical estimations of $((32+26)\times5-26)\,bp\times0.34\,nm\,bp^{-1}=89.8$ nm, and 2.6 nm/helix×(6×2)helix+1.5 nm×5=38.7 nm, if we assigned a diameter of 2.6 nm per helix and a buckling gap between the tiles of 1.5 nm in aqueous media.[4a] The yield of perfect 5×6 patches of cDAO-c64nt-O can be estimated to be about 30% from the strength of the band on the agarose gel (Figure S16) and about 28% through statistical analysis of the occupancy area in the AFM images (Figure S24).

Because the asymmetric tile of acDAO-c64nt is as stable and rigid as the symmetric tile of cDAO-c64nt, the predictable curvature of acDAO-c64nt results in formation of curved acDAO-c64nt-E (-E was designed as linear connections in Figure S13) nanowires, including nanorings, nanoarcs, and nanospirals (Figure 3D, H). Statistically, the one-tile-wide curved nanowires are mostly composed of 10 to 20 tiles. From the well-known worm-like chain model, the rigidity of a polymer can be characterized quantitatively by the persistence length along the polymer longitudinal axis. We applied the open-source software FiberApp[13] to estimate the persistence length of acDAO-c64nt-E at about 700 nm (details are given in section 2 of the Supporting Information), which is 14 times the persistence length of a linear double-helix of 50 nm. This value is reasonable because it is in agreement with the rigid and straight rod model of the (a)cDAO-c64nt tile, and comparable to the previously reported persistence length in the range of 2.0 to 30.0 μm for nanotubes composed of DAE-E and DNA origami.[10,14]

The AFM images and schematic assembling models of two-tile infinite lattices of cDAO-c84nt-E and cDAO-c84nt-O are shown in Figure 4A, B, D, and E, respectively. cDAO-c84nt-E requires all tiles to be aligned identically, which results in uniform nanotubes with a diameter of 120 nm; this corresponds to 24 cDAO-c84nt tiles rolled up with zigzag connections. Unlike the rigid and planar cDAO-c64nt tiles assembling into nanoribbons, cDAO-c84nt possesses a curved face and two asymmetric growth axes along its two crossed sides, which lead to the closure of the tile array to form a nanotube, similar to the linear DAE-E system.[10] The double-layered nanotube is 2.5 nm high and 5–15 μm long (Figures 4A and S21). Theoretically, the lattice unit cell should correspond to a rhombus with a side length of $(32+21)\,bp\times0.34\,nm\,bp^{-1}=18.0$ nm. However, careful measurements from open nanotubes confirm that the unit cell is a parallelogram, with an acute interior angle of 69° and two side lengths of 18.3 and 16.2 nm (Figures 4A, D and S21). The parallelogram lattice is certainly attributed to the secondary and tertiary tile structure of cDAO-c84nt, the detailed chiral model of which is suggested to be a pair of two congruent hollow triangles forming a crossed quadrilateral (Figure 4D, F), with two parallel bases tilted 70.9° towards the horizontal (Figure S5).

The chirality of cDAO-c84nt is attributed to the synergistic effect of the central HJ in combination with four three-way junctions. Of the five junctions, the central HJ plays the main role in alignment.[5d] The measured interior angle of the parallelogram lattice of 69°, which is larger than the apex angle of 54.2° in the suggested model (Figure S5), indicates that the unit cell of the apparent parallelogram is actually a polygon, and 69° is a collective angle obtained by simplifying the polygon into a parallelogram. The absolute tile conformation in cDAO-c84nt-E, including its chirality and the rotation direction of c84nt, can be deduced directly from its lattice structure; thus the red and green connected strands in Figure 4D are assigned to the right- and left-handed, respectively, twisting nets of the nanotube in Figure 4A. cDAO-c84nt-O follows the corrugation folding rule; therefore, planar nanoribbons, accompanied by nanotubes, were easily obtained (Figures 4B, E and S22). The formation of nanotubes is similar to that in the linear DAE-O system,[1b] because the folding of a planar lattice to a nanotube is thermodynamically favored. In view of the lattice

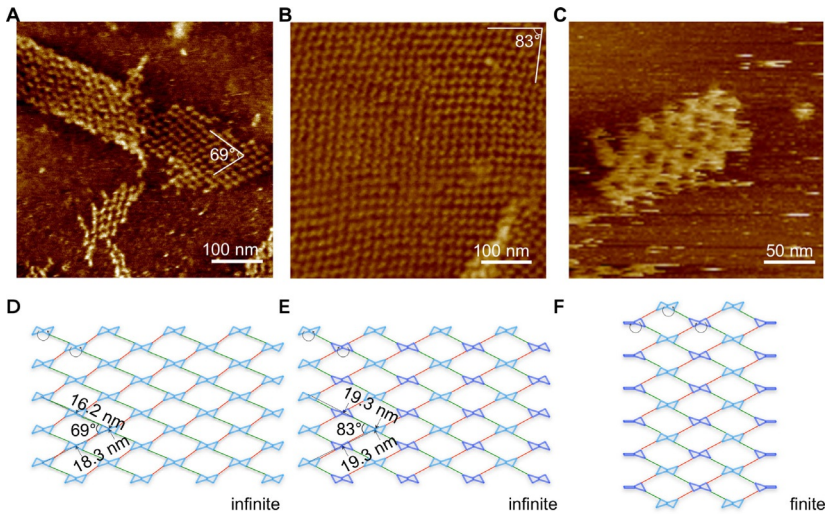

Figure 4. AFM images of A) infinite cDAO-c84nt-E, B) infinite cDAO-c84nt-O, C) finite 5×6 patches of cDAO-c74&c84nt-O, and their corresponding tile assembly models (D–F). The finite lattice of cDAO-c74&c84nt-O (C and F) contains 12 asymmetric cDAO-c74nt tiles, distributed on both the left and right sides, and 20 cDAO-c84nt tiles inside. The schematic cDAO-c84nt tile core model in (D)–(F) is represented as a pair of two congruent hollow triangles that form a crossed quadrilateral, the left and right sides of which are tilted 70.9° towards the horizontal (Figure S5); the schematic asymmetric cDAO-c74nt tile core model in (F) is represented with half of a hollow triangle and half of a solid parallelogram. The lattice parameters are labeled on the assembly models of (D) and (E). In (D)–(F), curved arrows indicate the rotation directions of circular scaffolds; the intertile connections are labeled as red and green segments; and the two different faces of cDAO-c84nt are distinguished as sky blue and deep blue, respectively; schematic cDAO-c84nt and cDAO-c74nt tiles are aligned with horizontal longitudinal axes.

strength, cDAO-c84nt is not as rigid as cDAO-c64nt, and the intertile connections are spatially isolated; thus the whole cDAO-c84nt-O lattice is much softer, and can be rolled randomly into nanotubes with nonuniform diameters. The planar nanoribbons are 0.5–3.0 μm wide and 2–5 μm long (Figure S22). The rhombic lattice constant is 19.3 nm, which is in agreement with the theoretical length of $(32+26)\,bp\times0.34\,nm\,bp^{-1}=19.7$ nm. The acute interior angle of the rhombic unit cell is 83°. From the corrugation rule, both upper and lower surfaces of a cDAO-c84nt-O ribbon are structurally equal.

To demonstrate their affordable assembly diversities, a finite lattice of 5×6 patches of cDAO-c74&c84nt-O (sequences in Figure S15) is shown in Figure 4C and F. The lattice was measured to be about 150.0 nm long and about 60.0 nm wide, which corresponded to theoretical estimations of $(32+26)\,bp\times0.34\,nm\,bp^{-1}\times\sin(83^\circ/2)\times12=156.8$ nm and $(32+26)\,bp\times0.34\,nm\,bp^{-1}\times\cos(83^\circ/2)\times4=59.1$ nm, respectively. All four edges end with six protruding thymine overhangs. To intensify both edges along the horizontal, we used the asymmetric tile of cDAO-c74nt, which carries half of a hollow triangle and half of a solid parallelogram (Figure 4F), and set the half-parallelogram towards the outside. In this finite lattice, only one c84nt strand was used as the scaffold of all 20 cDAO-c84nt tiles, and one c74nt strand was used as the scaffold of all 12 cDAO-c74nt tiles; whereas the sequences of all overhangs were designed to be specifically different for intertile connections. The yield for the comparably sized 5×6 patches of cDAO-c74&c84nt-O can be estimated to be about 23.5% from the strength of the band on an agarose gel (Figure S16).

In summary, structural polymorphism of mono- and polymers of fully associated c64nt or c84nt, with a central HJ and a pair of two central symmetric nicks, was found through native PAGE results. Using a new type of cDAO tiles of cDAO-c64nt, cDAO-c74nt, and cDAO-c84nt, we successfully obtained perfect 2D lattices of planar nanoribbons and nanotubes through even and odd half-turns intertile connections, respectively. The visible lattice structures and corresponding invisible molecular structures of HJs, inclination angle, and tile chirality can be correlated very well. The high rigidity of twin tiles of cDAO-c64nt and acDAO-c64nt was probed by native PAGE, with a surprisingly fast migration speed, and by AFM imaging, with densely textured planar nanoribbons for cDAO-c64nt-E(O) and curved nanowires with a persistence length of about 700 nm for acDAO-c64nt-E. The topological constraint should be the main parameter considered in the construction of DNA motifs and lattices by using circular DNA tiles instead of linear ones. This work illustrates some advantages of circular tiles for DNA nanotechnology.

Acknowledgements

We are grateful for financial support from the NSFC (grants no. 91753134 and 21571100), and the State Key Laboratory of Bioelectronics of Southeast University.

Conflict of Interest

The authors declare no conflict of interest.

Keywords: DNA structures · nanotechnology · noncovalent interactions · self-assembly · structure elucidation

[1] a) F. Tsu-Ju, N. C. Seeman, *Biochemistry* **1993**, *32*, 3211 – 3220; b) E. Winfree, F. Liu, L. A. Wenzler, N. C. Seeman, *Nature* **1998**, *394*, 539 – 544; c) F. Liu, R. Sha, N. C. Seeman, *J. Am. Chem. Soc.* **1999**, *121*, 917 – 922.

[2] a) H. Yan, S. H. Park, G. Finkelstein, J. H. Reif, T. H. LaBean, *Science* **2003**, *301*, 1882 – 1884; b) D. Liu, M. Wang, Z. Deng, R. Walulu, C. Mao, *J. Am. Chem. Soc.* **2004**, *126*, 2324 – 2325; c) Y. He, Y. Tian, Y. Chen, Z. Deng, A. E. Ribbe, C. Mao, *Angew. Chem. Int. Ed.* **2005**, *44*, 6694 – 6696; *Angew. Chem.* **2005**, *117*, 6852 – 6854; d) C. Tian, X. Li, Z. Liu, W. Jiang, G. Wang, C. Mao, *Angew. Chem. Int. Ed.* **2014**, *53*, 8041 – 8044; *Angew. Chem.* **2014**, *126*, 8179 – 8182; e) P. Wang, S. Wu, C. Tian, G. Yu, W. Jiang, G. Wang, C. Mao, *J. Am. Chem. Soc.* **2016**, *138*, 13579 – 13585.

[3] a) Y. Ke, L. L. Ong, W. M. Shih, P. Yin, *Science* **2012**, *338*, 1177 – 1183; b) B. Wei, M. Dai, P. Yin, *Nature* **2012**, *485*, 623 – 626; c) Y. Ke, L. L. Ong, W. Sun, J. Song, M. Dong, W. M. Shih, P. Yin, *Nat. Chem.* **2014**, *6*, 994 – 1002; d) B. Wei, L. L. Ong, J. Chen, A. S. Jaffe, P. Yin, *Angew. Chem. Int. Ed.* **2014**, *53*, 7475 – 7479; *Angew. Chem.* **2014**, *126*, 7605 – 7609.

[4] a) P. W. K. Rothemund, *Nature* **2006**, *440*, 297 – 302; b) S. M. Douglas, H. Dietz, T. Liedl, B. Högberg, F. Graf, W. M. Shih, *Nature* **2009**, *459*, 414 – 418; c) H. Dietz, S. M. Douglas, W. M. Shih, *Science* **2009**, *325*, 725 – 730; d) A. Aghebat Rafat, T. Pirzer, M. B. Scheible, A. Kostina, F. C. Simmel, *Angew. Chem. Int. Ed.* **2014**, *53*, 7665 – 7668; *Angew. Chem.* **2014**, *126*, 7797 – 7801; e) F. Hong, S. Jiang, T. Wang, Y. Liu, H. Yan, *Angew. Chem. Int. Ed.* **2016**, *55*, 12832 – 12835; *Angew. Chem.* **2016**, *128*, 13024 – 13027.

[5] a) R. Holliday, *Genet. Res.* **1964**, *5*, 282 – 304; b) D. R. Duckett, A. I. H. Murchie, R. M. Clegg, A. Zechel, E. von Kitzing, S. Diekmann, D. M. J. Lilley, *Struct. Methods, Hum. Genome Initiat. DNA Recomb.* **1990**, *1*, 157 – 181; c) M. Ariyoshi, D. G. Vassylyev, H. Iwasaki, H. Nakamura, H. Shinagawa, K. Morikawa, *Cell* **1994**, *78*, 1063 – 1072; d) B. F. Eichman, J. M. Vargason, B. H. Mooers, P. S. Ho, *Proc. Natl. Acad. Sci. USA* **2000**, *97*, 3971 – 3976.

[6] a) D. Ackermann, T. L. Schmidt, J. S. Hannam, C. S. Purohit, A. Heckel, M. Famulok, *Nat. Nanotechnol.* **2010**, *5*, 436 – 442; b) D. Ackermann, S. S. Jester, M. Famulok, *Angew. Chem. Int. Ed.* **2012**, *51*, 6771 – 6775; *Angew. Chem.* **2012**, *124*, 6875 – 6879; c) F. Lohmann, D. Ackermann, M. Famulok, *J. Am. Chem. Soc.* **2012**, *134*, 11884 – 11887; d) H. Zheng, M. Xiao, Q. Yan, Y. Ma, S. J. Xiao, *J. Am. Chem. Soc.* **2014**, *136*, 10194 – 10197; e) M. Wang, H. Huang, Z. Zhang, S.-J. Xiao, *Nanoscale* **2016**, *8*, 18870 – 18875; f) A. Noshin, M. Ali, M. Wang, M. M. F. A. Baig, S.-J. Xiao, *Nanoscale* **2017**, *9*, 17181 – 17185.

[7] W. Wang, T. Lin, S. Zhang, T. Bai, Y. Mi, B. Wei, *Nucleic Acids Res.* **2016**, *44*, 7989 – 7996.

[8] a) S. I. Nakano, D. Miyoshi, N. Sugimoto, *Chem. Rev.* **2014**, *114*, 2733 – 2758; b) A. Bhattacherjee, Y. Levy, *Nucleic Acids Res.* **2014**, *42*, 12415 – 12424; c) M. Wang, N. Afshan, B. Kou, S. J. Xiao, *ChemNanoMat* **2017**, *3*, 740 – 744.

[9] a) P. G. de Gennes, *J. Chem. Phys.* **1971**, *55*, 572 – 579; b) G. W. Slater, J. Noolandi, *Phys. Rev. Lett.* **1985**, *55*, 1579 – 1582; c) G. W. Slater, J. Noolandi, *Biopolymers* **1989**, *28*, 1781 – 1791; d) S. D. Levene, B. H. Zimm, *Science* **1989**, *245*, 396 – 399; e) D. M. J. Lilley, *Q. Rev. Biophys.* **2008**, *41*, 1 – 39.

[10] P. W. K. Rothemund, A. Ekani-Nkodo, N. Papadakis, A. Kumar, D. K. Fygenson, E. Winfree, *J. Am. Chem. Soc.* **2004**, *126*, 16344 – 16352.

[11] O. Kennard, W. N. Hunter, *Angew. Chem. Int. Ed. Engl.* **1991**, *30*, 1254 – 1277; *Angew. Chem.* **1991**, *103*, 1280 – 1304.

[12] C. Geary, P. W. K. Rothemund, E. S. Andersen, *Science* **2014**, *345*, 799 – 804.

[13] I. Usov, R. Mezzenga, *Macromolecules* **2015**, *48*, 1269 – 1280.

[14] a) D. Schiffels, T. Liedl, D. K. Fygenson, *ACS Nano* **2013**, *7*, 6700 – 6710; b) A. M. Maier, W. Bae, D. Schiffels, J. F. Emmerig, M. Schiff, T. Liedl, *ACS Nano* **2017**, *11*, 1301 – 1306.

Manuscript received: March 6, 2018

Accepted manuscript online: April 12, 2018

Version of record online: May 30, 2018